The Astrophysical Journal, 577:974–985, 2002 October 1

TITANIUM AND VANADIUM CHEMISTRY IN LOW-MASS DWARF STARS

Katharina Lodders
Planetary Chemistry Laboratory, Department of Earth and Planetary Sciences, Washington University, Campus Box 1169, Saint Louis, MO 63130-4899; lodders@levee.wustl.edu
Received 2002 April 23; accepted 2002 June 8

ABSTRACT

The equilibrium gas and condensation chemistry of titanium and vanadium in M, L, and T dwarf atmospheres is computed. The calcium titanates ($Ca_3Ti_2O_7$ and $Ca_4Ti_3O_{10}$) are identified for the first time as important Ti-bearing condensates in addition to perovskite ($CaTiO_3$) and Ti oxides in dwarf atmospheres. The chemistry of Ti is intimately coupled to that of refractory condensates containing Ca and Al, whose chemistry is much more intricate than commonly assumed. The TiO gas abundances in equilibrium with $Ca_3Ti_2O_7$ or $Ca_4Ti_3O_{10}$ are lower than the TiO gas abundances in equilibrium with perovskite. Consequently, this implies that TiO opacities are lower than previously assumed at temperatures and pressures where the new Ca titanates are stable. Vanadium condenses into solid solution with Ti-bearing condensates (as observed in meteorites) and not as "pure" vanadium oxide, as commonly assumed. The calculated TiO (gas) and VO (gas) abundances are used to constrain temperatures at the M/L dwarf transition. Adopted temperatures are 2010 K (with an upper limit of 2245 K) for M8 and 1960 K for M9. Temperatures at the beginning of the L sequence are less than 1950 K and are tentatively placed at ~1910 K for L0.

Subject headings: astrochemistry — stars: fundamental parameters — stars: late-type — stars: low-mass, brown dwarfs

1. INTRODUCTION

Low-mass dwarf stars and brown dwarfs possess cool atmospheres with effective temperatures ranging from $T_{\rm eff} \sim 2500$ K in late-M dwarfs to ~800 K in Gl 570D, one of the coolest brown dwarfs currently known (e.g., Geballe et al. 2001). The lower the temperature, the more molecular chemistry manifests itself in the observable parts of dwarf atmospheres. The appearance of certain molecular bands serves as a diagnostic for the new L and T dwarf classification (Kirkpatrick et al. 1999; Martin et al. 1999; Burgasser et al. 2002; Geballe et al. 2002). As discussed by Lodders (1999), the presence of certain molecules can serve as a proxy of temperature (T), because chemical species depend on temperature, but the effects of total pressure ($P_{\rm tot}$) also have to be considered. The most profound effect of a decrease in temperature is that carbon monoxide (CO) converts to methane (CH_4) around 1300–1500 K, depending on $P_{\rm tot}$ (e.g., Lodders & Fegley 2002). This switch defines the beginning of the T dwarf regime with the onset of methane absorption in the K and H bands (Kirkpatrick et al. 1999, 2000; Martin et al. 1999; Geballe et al. 2002).

Spectra of early-L dwarfs more closely resemble those of M dwarfs, but with decreasing temperature TiO and VO bands weaken, while atomic alkali lines and water (H_2O) and metal hydride (FeH and CrH) bands increase in strength in optical and near-IR spectra. In M dwarfs, TiO and VO are major opacity sources in the optical, and their weakening makes the atmosphere more transparent so that hydride bands and monatomic alkali lines become prominent in the spectra of L dwarfs. Thus, the gradual disappearance of TiO and VO bands and strengthening of hydride (FeH and CrH) bands marks the transition from M to L dwarfs (Kirkpatrick et al. 1999, 2000; Martin et al. 1999).

Within the L sequence some of the spectral features eventually pass through a "maximum" in strength and then decline, which is used to characterize the L subclasses (see Kirkpatrick et al. 1999, 2000; Martin et al. 1999). The details of these two classification schemes are still under debate, and amendments to these schemes (such as modifying and adding optical indexes and/or introducing infrared spectral indexes) are proposed (e.g., Geballe et al. 2002). Whatever the details of the classifications may become, the underlying principle utilized by all classification schemes is that (1) chemistry is going on in the atmospheres, which determines the spectral features, and (2) chemistry, which is temperature dependent, somehow enters into the subclassification of dwarfs.

Generally, decreasing temperatures favor formation of neutral atoms from their respective ions, molecule formation from constituent atoms, and condensation of gases into solids and liquids. This behavior is well known for the alkali metals, which replace their respective ions within the M/L dwarf sequence. Decreases in atomic alkali line strengths within the L and T dwarf sequence reflect formation of molecular alkali gases such as chlorides and other halides, hydroxides, and hydrides from the monatomic alkali gases as temperature drops (Lodders 1999). In addition to molecular gases, condensates are important for understanding decreases in line or band strengths. For example, within the L and T sequences, spectral features of Na, K, FeH, and CrH weaken because Na is removed by condensation of Na_2S (solid), K disappears into KCl (gas) and then into KCl (solid), and Fe and Cr are removed by metal condensation at lower T.

The topic of this paper is the equilibrium chemistry of Ti and V. This is important because TiO and VO bands are used in the L classification. Their presence is a typical characteristic of M dwarfs, where bands of VO and TiO are strongest in the optical spectra up to around M8–M9, where their bands begin to weaken (Jones & Tsuji 1997; Kirkpatrick et al. 1999, 2000; Martin et al. 1999). The TiO and VO bands decrease further through the L sequence and are essentially absent in the coolest L dwarfs and T dwarfs. The

decrease in band strength is associated with reduction of TiO and VO abundances by formation of other molecular gases (TiO_2 and VO_2) and by removal of Ti and V into condensates. Condensation of Ti and V in solid solution with perovskite ($CaTiO_3$) in brown dwarf atmospheres was described by Fegley & Lodders (1996) shortly after Nakajima et al. (1995) discovered the first brown dwarf Gl 229B. The importance of dust formation in cool dwarfs was also noted at about the same time by Tsuji and coworkers (Tsuji, Ohnaka, & Aoki 1996a; Tsuji et al. 1996b; Jones & Tsuji 1997), although their earlier models did not include any Ti- and V-bearing condensates. The Ti chemistry in models by Burrows & Sharp (1999) and by Allard et al. (2001) concur with our earlier identification of perovskite as the initial Ti-bearing condensate in cool dwarf atmospheres. As discussed below, three oxides, Ti_2O_3, Ti_3O_5, and Ti_4O_7, are also stable condensates, but the T and P conditions at which they appear are different than previously reported in the literature.

This paper shows that two other calcium titanates ($Ca_3Ti_2O_7$ and $Ca_4Ti_3O_{10}$) are important Ti-bearing condensates in dwarf atmospheres. The TiO (gas) abundances in equilibrium with either of these two titanates is significantly less than that in equilibrium with $CaTiO_3$. As a result, the TiO (gas) opacity should be significantly lower because less TiO remains in the gas if $Ca_3Ti_2O_7$ or $Ca_4Ti_3O_{10}$ condense instead of $CaTiO_3$. Furthermore, the chemistry of refractory condensates containing Ca and Al is not as simple as commonly assumed within these atmospheres. For example, several authors adopt corundum (Al_2O_3) as the first Al-bearing condensate at all total pressures, but calcium aluminates such as hibonite ($CaAl_{12}O_{19}$), grossite ($CaAl_4O_7$; also called calcium dialuminate), and gehlenite ($Ca_2Al_2SiO_7$) replace corundum as the initial condensate with increasing total P_{tot} (see Fig. 2 in Lodders 1999; Kornacki & Fegley 1984). Correct treatment of Ca and Al condensation is needed because the equilibrium chemistries of Ti, Ca, and Al are inextricably linked together. In turn, the condensation chemistry of titanium is important for that of vanadium because Ti-bearing condensates serve as host phases for vanadium condensation.

The paper is organized as follows. The computational methods are outlined in § 2. Titanium condensation at constant total pressure is described in § 3, followed by the discussion of Ti condensate stability as function of T and variable P_{tot} in § 4. A comparison of the Ti chemistry to other results in the literature is given in § 5. The TiO gas abundances as a function of T and P_{tot} are presented in § 6. The vanadium chemistry is given in § 7. The results are used to estimate temperatures at the M/L dwarf transition in § 8. Conclusions are summarized in § 9.

2. COMPUTATIONAL METHODS

Chemical equilibrium computations were done using the CONDOR code, which is described in detail elsewhere (e.g., Fegley & Lodders 1994; Lodders & Fegley 2002). The calculations are for solar composition using the selected solar elemental abundances given in Table 2.2 of Lodders & Fegley (1998). Among the ~2100 gases for compounds of all naturally occurring elements in the computations, 29 Ti-bearing and 16 V-bearing gases are considered; among them are Ti, Ti^+, Ti^-, TiC_2, TiC_4, TiO, TiO^+, TiO_2, TiS, V, V^+, V^-, VC, VC_2, VN, VO, VO_2, and VS, as well as Ti and V halides and oxyhalides. Among Ti-bearing solid and liquid condensates are $CaTiO_3$, $Ca_3Ti_2O_7$, $Ca_4Ti_3O_{10}$, TiO, TiO_2 (rutile), Ti_2O_3, α- and β-Ti_3O_5, Ti_4O_7, $CaTiSiO_5$ (titanite), TiS, TiS_2, Ti halides, Al_2TiO_5, $MgTiO_3$ (geikielite), $MgTi_2O_5$, Mg_2TiO_4, $FeTiO_3$ (ilmenite), Fe_2TiO_4 (ulvospinel), $MnTiO_3$ (pyrophanite), Mn_2TiO_4, and titanates of less abundant elements (e.g., Ba, Co, Ni, Pb, Sr, and Zn). The V-bearing condensates include VO, VO_2, V_2O_3, V_2O_4, V_2O_5, V_3O_5, V_4O_7, Ca vanadates, and V halides. An effort was made to include as many as possible solids and liquids of rock-forming elements for which reliable thermodynamic properties exist. The high-temperature condensates in meteorites serve as a guide to the initial condensates expected, and many of these minerals are included here. In addition, many other phases are included because conditions in low mass object atmospheres are different than those of meteoritic mineral formation (see § 4). Mineral names, ideal chemical formulae, and melting points relevant for the discussion below are listed in Table 1. The computations use the thermodynamic database maintained at the Planetary Chemistry Laboratory (see Lodders & Fegley 2002), for which thermochemical properties are routinely and continuously upgraded. Calculations were done from 1000–3000 K and 10^{+3} to 10^{-3} bars total pressure.

TABLE 1
CONDENSATE PROPERTIES

Condensate Name	Ideal Formula	Melting Point (K)
Perovskite	$CaTiO_3$	2188
Ca titanate	$Ca_4Ti_3O_{10}$	2078[a]
Ca titanate	$Ca_3Ti_2O_7$	2013[a]
Ti oxide	Ti_2O_3	2115
Ti oxide	Ti_3O_5	2050
Ti oxide	Ti_4O_7	1950
Corundum	Al_2O_3	2327
Hibonite	$CaAl_{12}O_{19}$	2106
Grossite	$CaAl_4O_7$	2038
Gehlenite	$Ca_2Al_2SiO_7$	1866
Akermanite	$Ca_2MgSi_2O_7$	1731
Spinel	$MgAl_2O_4$	2408
Forsterite	Mg_2SiO_4	2174
Enstatite	$MgSiO_3$	1850

[a] Melts incongruently to Ca-Ti–oxide melt plus perovskite (solid).

3. TITANIUM CHEMISTRY AT 1 BAR TOTAL PRESSURE

In order to facilitate the discussion of the Ti equilibrium chemistry as a function of T and P_{tot} in § 4, its temperature dependence at constant P of 1 bar (10^6 dyn cm^{-2}) is described first. The distribution of Ti between gases and condensates is shown in Figure 1*a*, and the corresponding graph for Ca is in Figure 1*b*. These two figures are discussed together next, because the Ti and Ca chemistries are linked.

We follow the chemistries from high to low temperatures. At the highest temperatures shown (2150 K), Ti is mainly

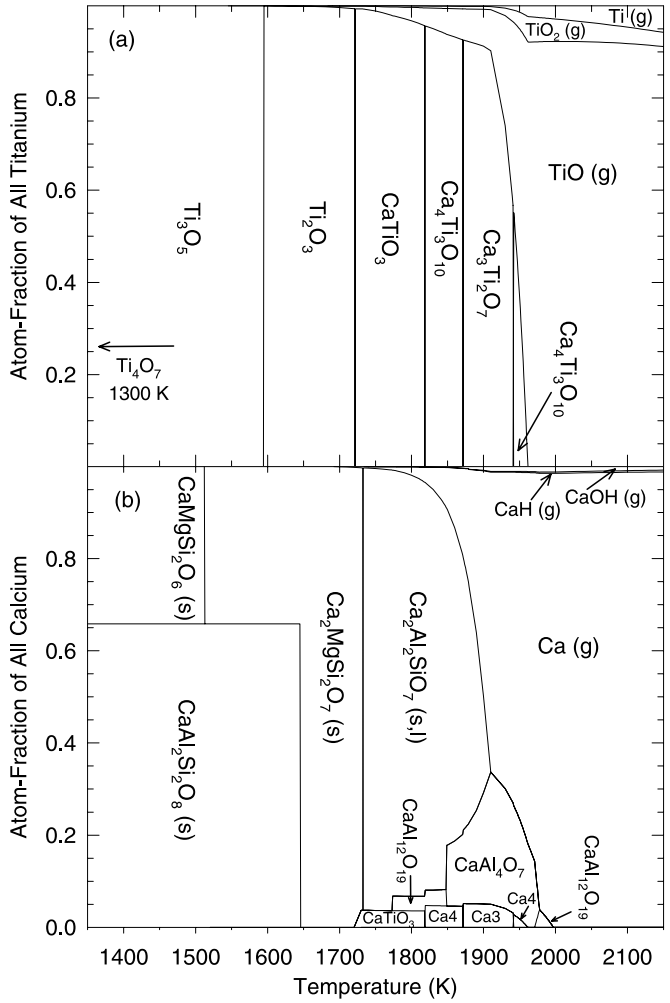

FIG. 1.—Distribution of (*a*) titanium and (*b*) calcium between condensates and gases as a function of temperature at 1 bar total pressure. Plotted are atom fractions contained in each phase. The first stable condensates are $Ca_4Ti_3O_{10}$ and $CaAl_{12}O_{19}$. Condensation temperatures are given in Table 2. The names of Ca titanates are abbreviated as Ca4 = $Ca_4Ti_3O_{10}$ and Ca3 = $Ca_3Ti_2O_7$ in (*b*). Except for gehlenite, which is liquid above its melting point of 1866 K, all condensates are solid at 1 bar.

present as TiO (gas). The two other major Ti-bearing gases are TiO_2 and monatomic Ti. Other Ti-bearing gases are not nearly as abundant and make up less (0.05%) of all Ti. At higher T than shown, atomic Ti (gas) increases at the expense of TiO (gas), and near 3000 K all Ti is about evenly distributed between TiO (gas) and Ti (gas). The next most abundant gases at 3000 K are TiO_2, containing 0.3% of all Ti, and Ti^+ and TiO^+, each containing ~0.1% of Ti.

Calcium gas chemistry at these high temperatures is dominated by monatomic Ca (gas). At 3000 K, ~96.2% of all Ca is in Ca (gas), followed by ~2.9% Ca^+, ~0.8% CaH, and ~0.1% CaOH. Other Ca gases are less important. At 2150 K in Fig. 1*b*, the percentages of Ca (gas) and CaOH (gas) are increased to ~98.9% and ~0.7%, respectively, while that of CaH (gas) has dropped to 0.4%. The abundance of Ca^+ (gas) is insignificant at 2150 K.

The highest temperature condensate containing either Ca or Ti is hibonite ($CaAl_{12}O_{19}$). It starts condensing at 1997 K but is replaced by grossite ($CaAl_4O_7$) at 1977 K. The replacement of hibonite with Ca : Al = 1 : 12 by grossite with Ca : Al = 1 : 4 occurs because most Ca is present as Ca (gas) at these temperatures. The net reaction

$$2\mathrm{Ca\ (gas)} + \mathrm{CaAl_{12}O_{19}\ (solid)} + 2\mathrm{H_2O\ (gas)} = 3\mathrm{CaAl_4O_7\ (solid)} + \mathrm{H_2\ (gas)} \quad (1)$$

proceeds to the right because grossite formation is favored by larger Ca (gas) abundances, all other factors being equal, according to the Le Chatelier–Braun principle.

The first Ti-bearing condensate, $Ca_4Ti_3O_{10}$ (solid), begins to form at 1963 K. It is replaced by $Ca_3Ti_2O_7$ (solid) at 1941 K, and the net reaction for this replacement is

$$\mathrm{Ca\ (gas)} + 2\mathrm{Ca_4Ti_3O_{10}\ (solid)} + \mathrm{H_2O\ (gas)} = 3\mathrm{Ca_3Ti_2O_7\ (solid)} + \mathrm{H_2\ (gas)}\,. \quad (2)$$

Reaction (2) is analogous to reaction (1) because in both cases the higher temperature mineral containing less calcium is replaced by a lower temperature mineral containing more calcium (e.g., $Ca_4Ti_3O_{10}$ [solid] with Ca : Ti = 1.33 : 1 and $Ca_3Ti_2O_7$ [solid] with Ca : Ti = 1.5 : 1).

Monatomic Ca (gas) becomes less abundant and eventually disappears with decreasing temperature as it is consumed by condensation of liquid and solid gehlenite. The major Ca-bearing phases are gehlenite, grossite, Ca (gas), and $Ca_3Ti_2O_7$ as T approaches 1871 K (Fig. 1). However, the competition of Ca-Al and Ca-Ti condensates for calcium exemplified by reactions (1) and (2) continues.

At 1871 K, $Ca_4Ti_3O_{10}$ reappears and consumes all the $Ca_3Ti_2O_7$. This could be interpreted as the reverse of reaction (2), but the Ca formed goes into gehlenite instead of being released back into the gas. Thus, gehlenite forms at the expense of $Ca_3Ti_2O_7$ and at the expense of $CaAl_4O_7$ via the reaction

$$3\mathrm{Ca\ (gas)} + \mathrm{CaAl_4O_7\ (solid)} + 2\mathrm{SiO\ (gas)} + 5\mathrm{H_2O\ (gas)} = 2\mathrm{Ca_2Al_2SiO_7\ (solid)} + 5\mathrm{H_2\ (gas)}\,, \quad (3)$$

which starts at 1908 K (1 bar). Reaction (3) decreases the thermodynamic activity of calcium to such a low value that $Ca_3Ti_2O_7$ becomes unstable and $Ca_4Ti_3O_{10}$ reappears.

Another consequence of gehlenite formation is that grossite is completely replaced by hibonite at 1848 K. This is a reversal of reaction (1) with the Ca that is generated being incorporated into gehlenite instead of going into the gas. Below 1848 K, gehlenite formation occurs at the expense of hibonite via the net reaction

$$11\mathrm{Ca\ (gas)} + \mathrm{CaAl_{12}O_{19}\ (solid)} + 6\mathrm{SiO\ (gas)} + 17\mathrm{H_2O\ (gas)} = 6\mathrm{Ca_2Al_2SiO_7\ (solid)} + 17\mathrm{H_2\ (gas)}\,. \quad (4)$$

The conversion of $Ca_4Ti_3O_{10}$ to perovskite ($CaTiO_3$) at 1818 K proceeds via the net reaction

$$\mathrm{Ca_4Ti_3O_{10}\ (solid)} + \mathrm{H_2\ (gas)} = 3\mathrm{CaTiO_3\ (solid)} + \mathrm{H_2O} + \mathrm{Ca\ (gas)}\,. \quad (5)$$

Reaction (5) is also a consequence of gehlenite formation because the calcium released by reaction (5) does not remain in the gas but is consumed by gehlenite via reaction (4). However, we can write separate equations for the formation of gehlenite and perovskite (or other Ti-bearing phases) because thermodynamics is path independent. Discussing the separate reactions makes it easier to see why the Ti

condensates replace one another and how the Ca-Al condensates and Ca-Ti condensates compete for calcium.

At 1818 K, where perovskite is stable, ~97% of all Ca and ~96% of all Ti are in solids, and the ~4% of Ti left is dominantly TiO (gas). Although perovskite contains less Ca than any other Ca titanate, it finally becomes unstable at 1720 K and is replaced by Ti_2O_3 (solid). The net reaction involved is

$$2CaTiO_3\ (\text{solid}) + 3H_2\ (\text{gas}) = Ti_2O_3\ (\text{solid}) + 3H_2O\ (\text{gas}) + 2Ca\ (\text{gas})\ . \quad (6)$$

The Ca released goes into akermanite ($Ca_2MgSi_2O_7$), the Mg-bearing end member of the gehlenite-akermanite solid solution. This solid solution becomes dominated by akermanite at 1732 K because the Al from the gehlenite and hibonite has gone into spinel, which becomes stable at 1774 K. Akermanite and spinel convert to diopside and anorthite, respectively, at lower temperatures. However, when these phases form, essentially all Al and Ca are already removed from the gas. Table 2 summarizes the sequence of Ca-, Al-, Ti-, and Mg-bearing condensates as a function of temperature at 1 bar pressure.

About 99.3% of all Ti is condensed, and only 0.7% remains in the gas at 1720 K, where Ti_2O_3 (solid) forms. This oxide is stable to 1594 K, where it is replaced by Ti_3O_5 (solid) via the net reaction

$$3Ti_2O_3 + H_2O = 2Ti_3O_5 + H_2\ . \quad (7)$$

In turn, Ti_3O_5 remains stable to 1300 K, where it is converted into Ti_4O_7 (solid) via the net reaction

$$4Ti_3O_5 + H_2O = 3Ti_4O_7 + H_2\ . \quad (8)$$

Reactions (6)–(8) involve changes in the oxidation state of titanium. The Ti in Ca_3TiO_3, $Ca_3Ti_2O_7$, and $Ca_4Ti_3O_{10}$ is tetravalent (Ti^{4+}), while Ca and O are both divalent (Ca^{2+} and O^{2-}). The conversion of perovskite to Ti_2O_3 by reaction (6) involves the reduction of Ti^{4+} to Ti^{3+} by hydrogen. In contrast, the conversion of Ti_2O_3 to Ti_3O_5 by reaction (7) involves oxidation of Ti^{3+} to Ti^{4+} because two of the Ti atoms in Ti_3O_5 are trivalent and one is tetravalent. Similarly, reaction (8) entails oxidation of Ti^{3+} because Ti_4O_7 contains two Ti^{4+} and two Ti^{3+} atoms. The driving force behind these reactions is discussed in § 4.

It should be noted that the Ca titanates $Ca_3Ti_2O_7$ and $Ca_4Ti_3O_{10}$ are more effective in removing TiO from the gas than perovskite. For illustration, if the condensates $Ca_3Ti_2O_7$ and $Ca_4Ti_3O_{10}$ are neglected in the computations and only perovskite is considered as a condensate, $CaTiO_3$ would remove ~29% of all Ti from the gas at 1950 K and 1 bar. If perovskite and $Ca_3Ti_2O_7$ are both included in the calculations, $Ca_3Ti_2O_7$ is stable instead of perovskite, and $Ca_3Ti_2O_7$ removes ~36% of all Ti. If all three titanates ($CaTiO_3$, $Ca_3Ti_2O_7$, and $Ca_4Ti_3O_{10}$) are included in the computations, as should be done, $Ca_4Ti_3O_{10}$ is the stable condensate at 1950 K and 1 bar, and it removes ~37% of the Ti from the gas. Thus, the thermodynamically most stable titanate is also the one removing most of the Ti from the gas. The condensation temperatures for the first Ti-bearing condensate do not change significantly if $Ca_3Ti_2O_7$, $Ca_4Ti_3O_{10}$, or perovskite are considered. At 1 bar the first condensate is $Ca_4Ti_3O_{10}$ (solid), with a condensation temperature of 1963 K. If this condensate and $Ca_3Ti_2O_7$ were neglected, perovskite would condense first at 1958 K, which is only 5 K less. Therefore, the temperatures where TiO gas removal starts are not that different in computations considering only perovskite or perovskite, $Ca_3Ti_2O_7$, and $Ca_4Ti_3O_{10}$. However, as discussed above, computations using only perovskite overestimate the remaining TiO gas abundances, which are indeed lower once all potential condensates are included.

TABLE 2
CONDENSATION SEQUENCE (K) AT DIFFERENT P_{tot}

	10 bars		1 bar		0.1 bars	
COMPOUND	In	Out	In	Out	In	Out
Hibonite.....	No	No	1997	1977	1912	1848
Grossite	2089	1959	1977	1848	1848	1751
Gehlenite	2039	1863	1908	1732	1796	1626
Hibonite.....	1959	1901	1848	1774	1751	1663
Spinel.....	1901	1746[a]	1774	1646[a]	1663	1560[a]
Akermanite.....	1863	1513[a]	1732	1513[a]	1626	1513[a]
Forsterite.....	1813	[b]	1698	[b]	1597	[b]
Enstatite	1721	[b]	1621	[b]	1534	[b]
$Ca_4Ti_3O_{10}$.....	No	No	1963	1941	1858	1818
$Ca_3Ti_2O_7$	2087	1988	1941	1871	1818	1768
$Ca_4Ti_3O_{10}$.....	1988	1948	1871	1818	1768	1707
Perovskite.....	1948	1913	1818	1720	1707	1610
Ti_2O_3	1913	1612	1720	1594	No	No
Ti_3O_5	1612	1349	1594	1300	1610	1290
Ti_4O_7	1349	[b]	1300	[b]	1290	[b]

[a] Spinel and akermanite convert to diopside and anorthite.
[b] Remains stable to lower end of computations (1000 K).

4. TITANIUM CONDENSATES AS A FUNCTION OF T AND P_{tot}

The stability of Ti-bearing condensates as a function of T and P_{tot} is illustrated in Figure 2. The axes on the plot are drawn so that T and P_{tot} increase toward the origin, to mimic T and P increases with depth into dwarf atmospheres. The thick lines show the T and P stability fields of the Ti-bearing condensates (*bold font*). The dotted lines (*italic*) mark the appearances of Ca- and Al-bearing condensates, enstatite ($MgSiO_3$), and forsterite (Mg_2SiO_4). The dash-dotted curve shows where methane and CO gas abundances are equal. The condensation temperatures and stability fields of the condensates discussed below are summarized for three different total pressures (0.1, 1, and 10 bars) in Table 2.

As discussed in § 3, the stabilities of Ca-Ti– and Ca-Al–bearing condensates influence each other. Whenever a new Ca-Al–bearing condensate becomes stable, a switch to another Ti-bearing condensate occurs within a small T interval. In addition to the T-dependence of the Ti condensate sequence, there is also a dependence on P_{tot}.

The condensation temperatures of most condensates increase with increasing P_{tot}. The first Ti-bearing condensate is always a Ca titanate: above $\log P_{tot} = +0.5$ it is $Ca_3Ti_2O_7$, between $\log P_{tot} = +0.5$ and -1.5 it is $Ca_4Ti_3O_{10}$, and at $\log P_{tot} < -1.5$ it is perovskite. In other words, higher P_{tot} favors formation of the titanate with the highest Ca : Ti ratio, which is $Ca_3Ti_2O_7$. At intermediate and lower P_{tot} values, titanates with lower Ca : Ti ratios form first, and temperatures have to drop to reach the stability field of $Ca_3Ti_2O_7$.

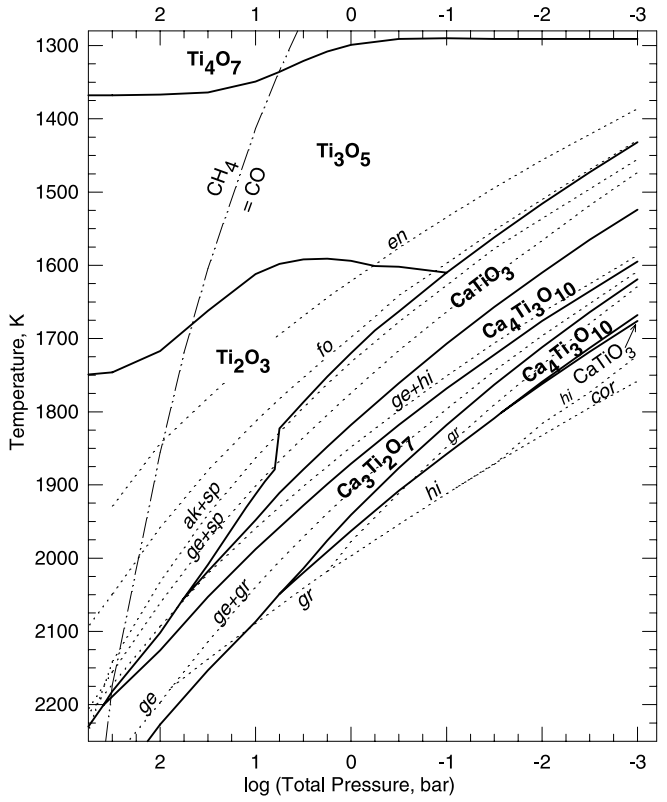

FIG. 2.—Stability fields of Ti-bearing condensates as a function of temperature and total pressure. Bold lines indicate stability boundaries of Ti-bearing condensates and dotted lines those of Ca- and Al-bearing ones. The dash-dotted line shows where CO (gas) abundances equal that of CH_4. Mineral names for Ti-free condensates are italic and abbreviated: *ak* = akermanite, *cor* = corundum, *en* = enstatite, *fo* = forsterite, *ge* = gehlenite, *gr* = grossite, *hi* = hibonite, and *sp* = spinel. Some of these condensates may be stable as liquids (see Table 1 for melting points). Condensation temperatures are given in Table 2. Note that temperature and total pressure increase toward the origin.

The Ca-Al–bearing condensates behave similarly, and at the highest P_{tot} more complex condensates are stable first. At the highest pressure shown, gehlenite is the first Ca-Al condensate. With decreasing P_{tot}, grossite, then hibonite, and finally corundum condense first (Kornacki & Fegley 1984; Lodders 1999). For example, at 10^{-3} bars, the lowest P_{tot} in Figure 2, the condensation sequence of Ca-Al minerals with decreasing T is corundum-hibonite-grossite-gehlenite. Figure 2 shows that in contrast to Ca-Ti minerals, two Ca-Al minerals can coexist for a limited T-interval. This point is also illustrated in Figure 1 and in Table 2. For example, if grossite is the first condensate and gehlenite condenses afterward, gehlenite coexists with grossite; if hibonite forms first or replaces grossite, hibonite coexists with gehlenite. The coexistence of two Ca-Al condensates is indicated in Figure 2 by two compound labels such as *ge* + *hi* and *ge* + *gr*. Not surprisingly, the location of the dual stability fields also influences the types of Ti-bearing condensates.

At the high-pressure end of Figure 2, $Ca_3Ti_2O_7$ is the first Ca titanate to form, but its stability with decreasing T is limited by the appearance of gehlenite, the Al-bearing end member of the melilite solid solution. The curve showing the onset of gehlenite formation passes right through the center of the $Ca_3Ti_2O_7$ stability field. Let us follow the Ti-bearing condensates at $\log P_{tot} < +1.5$, starting at temperatures where gehlenite coexists with grossite (*curve ge* + *gr*) and $Ca_3Ti_2O_7$. With decreasing T, a second, lower temperature stability field of the more Ca-poor $Ca_4Ti_3O_{10}$ appears because the gehlenite-dominated melilite solid solution consumes more Ca. This is the reason why grossite is replaced by the less Ca-rich aluminate hibonite shown by the curve *ge* + *hi* passing through the $Ca_4Ti_3O_{10}$ stability field. Eventually, $Ca_4Ti_3O_{10}$ becomes unstable and perovskite reappears, again because Ca is effectively sequestered into gehlenite. Hibonite stability ends and spinel stability begins (*curve ge* + *sp*) within this perovskite field. Finally, the melilite solid solution becomes dominated by its akermanite end member (*curve ak*+*sp*). At this point, essentially all Ca is in akermanite and all Al in spinel, and perovskite stability terminates shortly after akermanite appears.

Above $\log P_{tot} = +1.5$, the first titanate is also $Ca_3Ti_2O_7$ followed by $Ca_4Ti_3O_{10}$, but the "second," low-temperature perovskite stability field is barely reached. Compared to the low-pressure end of Figure 2, the stability of Ca titanates is more limited above $\log P_{tot} = +1.5$ because gehlenite, akermanite, and spinel consume Al and Ca at very high T. Thus, instead of moving through the condensation sequence present at lower P_{tot}, $Ca_4Ti_3O_{10}$ stability ends with the appearance of Ti_2O_3 at relatively high T.

The three stable Ti oxides with decreasing T are Ti_2O_3, Ti_3O_5, and Ti_4O_7 for $P_{tot} > 0.1$ bars. At lower P_{tot}, Ti_2O_3 is not stable, and perovskite is replaced by Ti_3O_5 instead. The Ti oxide formation sequence is caused by successive oxidation with decreasing T. As discussed earlier, all Ti in Ti_2O_3 is trivalent (Ti^{3+}), while Ti_3O_5 and Ti_4O_7 contain both Ti^{3+} and Ti^{4+}, with more Ti^{4+} in Ti_4O_7.

Reactions (7) and (8) proceed to the right at lower T because the H_2O/H_2 ratio increases with decreasing T as H_2O thermal dissociation and CO (gas) become less important (see Lodders & Fegley 2002 for details). Reactions (7) and (8) are independent of P_{tot} as long as the H_2O/H_2 ratio is constant. However, the H_2O/H_2 ratio and hence the Ti_2O_3/Ti_3O_5 and Ti_3O_5/Ti_4O_7 phase boundaries are influenced by the distribution of carbon between CH_4 and CO. This accounts for the unusual shape of the Ti_2O_3/Ti_3O_5 and Ti_3O_5/Ti_4O_7 boundaries. At high P_{tot}, where methane is the most abundant carbon gas, both Ti-oxide boundaries occur at higher T because there is less CO and more H_2O. The higher H_2O/H_2 ratio drives reactions (7) and (8) to the right. The conversion of CO to methane via the net thermochemical reaction $CO + 3H_2 = CH_4 + H_2O$ becomes increasingly important with increasing P_{tot} at constant T (Lodders & Fegley 2002). The gradual conversion of CO to CH_4 and H_2O takes place on the low-P side (where CO is more abundant) before the CO and CH_4 abundances are equal. This explains why the temperatures at the two Ti-oxide phase boundaries vary before the CH_4=CO boundary is reached.

In addition, the Ti_2O_3/Ti_3O_5 boundary shows a small dependence on P_{tot} between ~3 and 0.1 bars; e.g., at 1 bar, Ti_2O_3 stability extends to 1594 K, while at 0.1 bars, Ti_2O_3 is stable only to 1610 K. This behavior is caused by forsterite and enstatite condensation, which remove some water from the gas. Once the Al-, Ca-, Mg-, and Si-bearing minerals are fully condensed, ~15% of the total oxygen is tied up in rock. Most of this oxygen is consumed by Mg and Si, the two most abundant rock-forming elements. At 1 bar, forsterite and enstatite condense within the Ti_2O_3 stability field. Their

condensation slightly reduces the H_2O/H_2 ratio, and Ti_2O_3 stability is extended to lower T when compared to the case at 0.1 bars. At 0.1 bars, only forsterite condenses in the Ti_2O_3 field, leaving a comparably higher H_2O/H_2 ratio, which favors formation of the more oxidized Ti_3O_5 at higher T than at 1 bar.

The Ti-condensation chemistry is briefly summarized as follows: The first Ti-bearing condensate is always a Ca titanate, and with increasing P_{tot}, the sequence is perovskite, $Ca_4Ti_3O_{10}$, and $Ca_3Ti_2O_7$. The Ti oxides are stable after the titanates, when Ca is consumed by other condensates. The oxide condensation sequence is Ti_2O_3, Ti_3O_5, and Ti_4O_7, which reflects successive oxidation by the increased H_2O/H_2 ratio at lower T.

Previously, Mg-Ti oxides such as $MgTi_2O_5$ were reported to be stable by Burrows & Sharp (1999) and Allard et al. (2001). However, within the P-T range shown in Figure 2, Mg-Ti oxides are unstable. The formation of Mg-Ti oxides such as $MgTi_2O_5$ requires the presence of Mg in the gas. If Mg is removed into enstatite and forsterite condensate clouds at high T, Mg-Ti oxide formation is physically prevented in higher, cooler atmospheric regions. As noted elsewhere (Lodders 1999; Lodders & Fegley 2002), our cloud condensation models explain the presence of H_2S and GeH_4 and the absence of SiH_4 in Jupiter's atmosphere and the presence of monatomic K in brown dwarf atmospheres (see also Geballe et al. 2001). Our models can be tested by searching for SiH_4 (silane), which has very strong IR bands, in the atmospheres of T dwarfs. Silane should be absent above the Mg_2SiO_4 and $MgSiO_3$ clouds if our cloud condensation models are correct. Further aspects of cloud formation are not discussed here, and the interested reader is referred to Ackerman & Marley (2001).

The condensation sequence at higher total pressures in low-mass objects and the formation of cloud layers make it unlikely that the clinopyroxene diopside, condensing at relatively low temperatures (Fig. 1), incorporates Ti. The formation of Ti-bearing diopside from perovskite is expected in the condensation sequence of a solar composition gas at total pressures of $\leq 10^{-3}$ bars (see, e.g., Ebel & Grossman 2000). At $P_{tot} \leq 10^{-3}$ bars, Ti_2O_3 or Ti_3O_5 (see Fig. 2) do not form because Ti-bearing diopside forms instead. This requires not only lower total pressures but also that solid-solid-gas reactions are possible, which was the case in the solar nebula, where condensates remained more or less homogeneously dispersed in the gas. However, in low-mass objects Ti is sequestered in cloud layers deeper in the atmospheres, which means that formation of Ti-bearing diopside does not occur at lower temperatures. This illustrates that a comparison of the chemistry in low mass object atmospheres to the condensation record in meteorites and to the condensation chemistry under solar nebula conditions is limited because effects of total pressure and cloud formation alter the results for low mass object atmospheres.

Finally, it should be noted that the stability ranges of several condensates in Figure 2 extend to temperatures where condensates are present as liquids. The melting points of the condensates are given in Table 1. Gehlenite, akermanite, grossite, $Ca_3Ti_2O_7$, and $Ca_4Ti_3O_{10}$ are molten above 2000–2100 K, so the high-pressure end of Figure 2 is dominated by liquid condensates. The titanates melt incongruently to solid perovskite plus a Ca-Ti–oxide melt that persists until perovskite melts at 2188 K, above which a complete Ca-Ti–oxide melt exists. Such liquids typically have complex compositions and may be capable of dissolving other species, which needs further exploration.

5. COMPARISON OF Ti CHEMISTRY TO LITERATURE DATA

Titanium chemistry was also investigated by Burrows & Sharp (1999) and Allard et al. (2001). Except for differences at high P_{tot}, both groups find the condensation sequence perovskite-Ti_2O_3-Ti_4O_7 with decreasing temperature. There are several important differences between the present study and these two studies. Burrows & Sharp (1999) identify Ti_3O_5 as the first condensate in higher pressure, substellar objects with $T_{eff} > 2000$ K and $P_{tot} \sim< 10$ bars, and they also find that Ti_3O_5 coexists with $CaTiO_3$ within a small T-P range. This behavior is not found here, and here Ti_3O_5 is identified only as a lower T condensate (Fig. 2; Table 2). Allard et al. (2001) do not discuss this oxide, which probably means that they find that Ti_3O_5 does not form at all. The reason for the identification of Ti_3O_5 as an initial condensate at higher P and T by Burrows & Sharp (1999) is likely related to their thermodynamic data, which is described in the Appendix.

Here Ti_3O_5 is present between Ti_2O_3 and Ti_4O_7 (see Table 2), but neither Burrows & Sharp (1999) nor Allard et al. (2001) find this sequence. The sequential change in Ti oxidation state from all Ti^{3+} in Ti_2O_3, to two Ti^{3+} and one Ti^{4+} in Ti_3O_5, to two Ti^{3+} and two Ti^{4+} in Ti_4O_7 suggests that the oxide stability sequence here is more plausible. A possible explanation for the differences in the Ti-oxide chemistry could be the use of erroneous thermodynamic properties for Ti_3O_5 in the studies by Burrows & Sharp (1999) and Allard et al. (2001), as described in the Appendix. Ultimately, the validity of the present results for Ti condensation can be checked by modeling the opacity due to the predicted TiO (gas) abundances, which are discussed next.

6. TiO GAS ABUNDANCES AS A FUNCTION OF T AND P_{tot}

The discussion in the previous sections shows that there are ample Ti-bearing condensates capable of depleting TiO gas. The TiO (gas) mole fraction contours as a function of T and P_{tot} in Figure 3 were computed taking the presence of the different Ti condensates into account. The labeled contours give the log TiO mole fractions, and the dotted lines are spaced in 1 dex increments. The mole fraction X is defined as the partial pressure of TiO, $p(\mathrm{TiO})$, over the sum of all partial pressures; i.e., $X(\mathrm{TiO}) = p(\mathrm{TiO})/[p(\mathrm{H_2}) + p(\mathrm{He}) + p(\mathrm{H}) + p(\mathrm{H^+}) + p(\mathrm{H}) + p(\mathrm{H_2O}) + \ldots]$.

The shape and curvature of the TiO (gas) contours are due to the different Ti condensates present as a function of T and P_{tot} and to the effect of P_{tot} on the Ti gas phase chemistry at high T, where no Ti condensates are present. The discussion starts at the highest temperatures shown in Figure 3. The dash-dotted curve at the very bottom of Figure 3 shows where TiO and Ti have equal abundances. As discussed in § 3, TiO and Ti comprise about 99.5% of all Ti at about 3000 K. Thus, TiO and Ti each comprise about one-half of all titanium. The equal abundance contour is at ~3000 K, except at the lower pressure end of Figure 3, where it moves toward lower temperatures of 2800–2750 K.

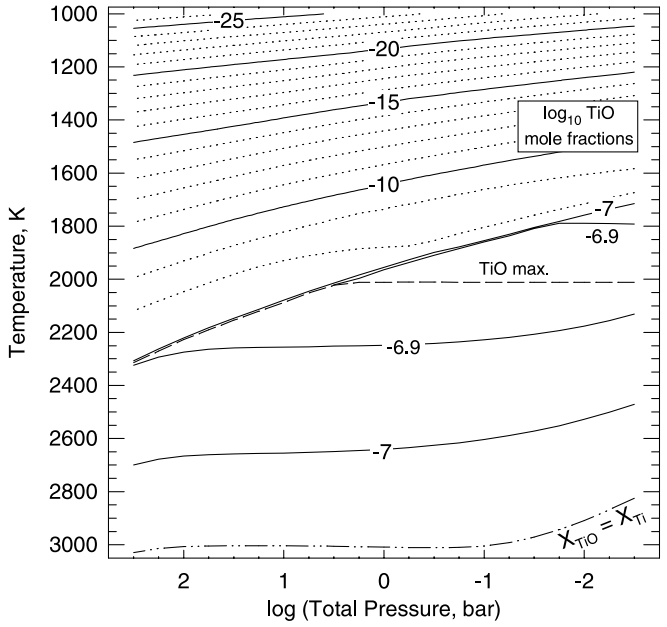

FIG. 3.—Mole fraction abundance contours (in $\log_{10}$ units) of TiO gas as a function of temperature and total pressure. See text for details.

At high T, where all titanium is in the gas, the abundance of TiO is controlled by the net thermochemical reactions

$$\mathrm{TiO_2\ (gas) + H_2\ (gas) = TiO\ (gas) + H_2O}\ , \qquad (9)$$

$$\mathrm{TiO\ (gas) + H_2\ (gas) = Ti\ (gas) + H_2O\ (gas)}\ , \qquad (10)$$

which both proceed to the right with increasing T. Reactions (9) and (10) are independent of $P_{\rm tot}$ as long as the H_2O/H_2 ratio is constant. The curvature in the contours for $X(\mathrm{TiO}) = X(\mathrm{Ti})$, $X(\mathrm{TiO}) = 10^{-7}$, and $X(\mathrm{TiO}) = 10^{-6.9}$ is due to the pressure-dependent changes in the H_2O/H_2 ratio (see Fig. 8*b* in Lodders & Fegley 2002). As mentioned earlier, changes in the H_2O/H_2 ratio are caused by H_2O thermal dissociation (more important at lower $P_{\rm tot}$) and to conversion of CO and CH_4 (more important at higher $P_{\rm tot}$). The curvature in the contours and the chemistry of H_2O in a solar composition gas described in detail by Lodders & Fegley (2002) are completely self-consistent.

As shown in Figure 3, TiO (gas) mole fractions increase with decreasing T and pass through a wide maximum where $X(\mathrm{TiO}) \sim 10^{-6.9}$. This behavior stems from the interplay of reactions (9) and (10): the former converting TiO to TiO_2 and the latter producing TiO from Ti. The dashed line labeled "TiO max." shows where the highest TiO mole fraction of $X(\mathrm{TiO}) \sim 10^{-6.88}$ is located. However, with increasing $P_{\rm tot}$ the "TiO max." contour intersects the Ca-titanate condensation curve (at $\log P_{\rm tot} = +0.5$, $P_{\rm tot} = 3.16$ bars).

Thus, at $\log P_{\rm tot} \geq +0.50$ the highest mole fraction of $\sim 10^{-6.88}$ is not reached because the maxima in TiO abundances coincide with the $Ca_3Ti_2O_7$ condensation temperatures. There are two contours for $X(\mathrm{TiO}) = 10^{-6.9}$ in Figure 3. The lower, high-temperature contour intersects and then closely follows the $Ca_4Ti_3O_{10}$ condensation temperature (within 1 K) only at the highest $P_{\rm tot}$ shown. The upper, lower temperature contour and that for $X(\mathrm{TiO}) = 10^{-7}$ intersect and follow the titanate condensation curve already at much lower $P_{\rm tot}$.

The TiO mole fractions drop in the T-P range where Ti condensates are stable because the TiO abundance is regulated by the vapor-solid chemical equilibria. For example, TiO mole fractions smaller than 10^{-10} are determined by the TiO vapor pressure over Ti_3O_5, i.e.,

$$\mathrm{Ti_3O_5\ (solid) = TiO\ (gas) + 2TiO_2\ (gas)}\ , \qquad (11)$$

and that over other Ti oxides.

7. VANADIUM CHEMISTRY

Vanadium is less refractory than titanium, but qualitatively, their gas chemistries are quite similar. The monoxide is the major gas prior to condensation for both elements. The neutral atom replaces the monoxide at high T, and the dioxide gains importance at low T. Despite the similarities in gas chemistry, the condensation chemistry of vanadium is quite different from that of Ti. If vanadium condenses into a "pure" V-bearing phase, VO (solid) would be the first condensate, which was also found by Burrows & Sharp (1999) and Allard et al. (2001). Calcium vanadates, which are analogous phases to the Ca titanates discussed above, are not stable. VO (solid) would form roughly 200 K lower than the first Ti-bearing condensates, reflecting the less refractory nature of vanadium.

However, vanadium is a trace element, and its abundance is only $\sim$10% of that of titanium. Trace elements are known to condense into solid solution with phases made up of more abundant elements instead of condensing as pure trace element compounds. For example, there are no pure vanadium compounds such as VO known to exist among the high-temperature condensate minerals in meteorites, but vanadium is often found as a trace constituent in phases such as perovskite and hibonite (for references, see Kornacki & Fegley 1986). Solid solution formation assumes that the trace element substitutes into a lattice position normally taken by a major element. As done previously (Kornacki & Fegley 1986; Fegley & Lodders 1996; Lodders 1999), condensation of vanadium is modeled here by assuming V substitutes of some of the Ti in Ti-bearing condensates. The computational procedure for condensation into solid solution is analogous to that described by Kornacki & Fegley (1986).

Condensation of V into solid solution starts when Ca titanates begin to form, and therefore the condensation temperatures where V-bearing condensates appear are the same as those for the Ca titanates. However, at a given T and $P_{\rm tot}$, the fraction of V removed from the gas is much less than the fraction of Ti removed; e.g., at 1900 K and 1 bar, 91% of all Ti is condensed, but only $\sim$10% of all V is sequestered into solid solution. Still, the net effect of solid solution formation is that VO gas removal begins at higher temperatures than in the case of "pure" VO condensation because vanadium condensation into solid solution starts as soon as a suitable host phase condenses.

The observed behavior of the VO and FeH bands in the red part of the optical spectra of late-M and early-L dwarfs supports modeling VO removal from the gas by solid solution formation instead of pure VO condensation. The disappearance of TiO, VO, and FeH bands within the spectral M/L sequence is generally believed to be caused by condensate formation. The VO bands begin to weaken around the M/L dwarf transition, while the FeH bands still grow stronger and reach their maximum strength around L3 and then

decrease with later (and presumably cooler) spectral type (Kirkpatrick et al. 1999; Martin et al. 1999). This suggests that VO (gas) is removed by condensation at higher temperatures than FeH (gas). However, iron metal condenses before "pure" VO (solid); e.g., at 1 bar, Fe condenses at 1834 K and VO at 1710 K. This implies that FeH bands should weaken in earlier spectral types before VO bands do, which is the opposite of what is observed. This inconsistency was not noted in the studies by Burrows & Sharp (1999) and Allard et al. (2001), who assumed condensation of pure VO. However, the only way to remove VO (gas) before FeH (gas) is to invoke V condensation into solid solution with Ti-bearing condensates, as done earlier (Fegley & Lodders 1996; Lodders 1999).

Figure 4 shows the mole fraction contours of VO gas for the same *T*-*P* grid used to show the mole fraction contours of TiO in Figure 3. The VO mole fractions decrease with decreasing temperatures once Ti-bearing condensates start forming (Fig. 4, *dashed curve* TC). The mole fraction contours for $\log X(\mathrm{VO}) = -8$ show that there is a relatively wide field for maximum VO abundances at $P_{\mathrm{tot}} < 1$ bar, which was also found for TiO abundances in Figure 3. The maximum VO gas abundances "VO max." of $\log X(\mathrm{VO}) \sim -7.99$ are at higher temperatures than Ca-titanate condensation only at $\log P_{\mathrm{tot}} < -1.5$. At higher P_{tot}, the maximum VO abundances coincide with the condensation temperatures of the Ca titanates. The TiO maximum abundance contour "TiO max." in Figures 3 and 4 also eventually coincides with the Ca titanate condensation temperatures but only at $\log P_{\mathrm{tot}} > +0.50$. Thus, TiO and VO abundance maxima occur at the same temperatures (coinciding with the Ca-titanate condensation *T*) at pressures larger than $\log P_{\mathrm{tot}} = +0.50$. Below $\log P_{\mathrm{tot}} = +0.50$, the maximum VO abundances occur at lower temperatures than the TiO maximum abundances, e.g., at 1960 K for VO and 2010 K for TiO at 1 bar. The VO mole fractions of $\geq 10^{-8}$ extend to lower temperatures even after condensation of Ca titanates occurs. This happens because VO is more volatile than TiO even if VO solid solution is considered (e.g., Kornacki & Fegley 1986).

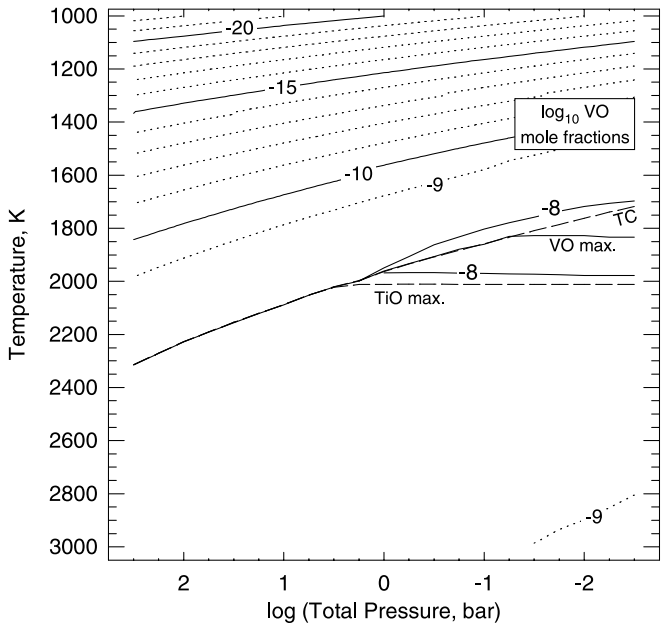

FIG. 4.—Mole fraction abundance contours (in $\log_{10}$ units) of VO gas as a function of temperature and total pressure. See text for details.

8. TEMPERATURES FROM CHEMISTRY AT THE M/L DWARF TRANSITION

The computational results can be used to find the temperatures near the M-to-L dwarf transition. Bands of TiO and VO reach maxima in the optical spectra for very late M dwarfs. According to Kirkpatrick et al. (1999) the maximum strength of TiO is around M7–M8 and that for VO around M9.5–L0. Martin et al. (1999) place the maximum for TiO at M8 and that for VO at M9, so the L sequence (L0) starts with declining TiO and VO band strengths. Here I use the placement of TiO and VO maxima according to the spectral assignments of Martin et al. (1999).

If TiO and VO band strengths in late-M and early-L dwarfs primarily reflect changes in oxide gas abundances, the maximum band strength corresponds to the maximum oxide abundance. Then we can find the corresponding temperatures for TiO and VO maxima from Figures 3 and 4. This approach assumes that other opacity sources such as water are not influencing TiO and VO band strengths in the red part (<1 μm) of the optical spectra for late-M and early-L dwarfs. It seems unlikely that such an effect is important for VO and TiO bands of these objects because one might expect that neighboring bands of TiO and VO (e.g., between 760 and 800 nm) would be affected in the same manner; i.e., additional opacity due to water would decrease both the TiO and VO bands simultaneously, which is at odds with TiO decreasing after M8 but VO only after M9.

In order to use Figures 3 and 4 to obtain a chemical temperature estimate, the total pressure needs to be constrained. The observation that the TiO and VO band strength maxima do not occur at the same spectral type indicates that total pressures in the band-forming region of M8 and M9 dwarfs must be smaller than $\log P_{\mathrm{tot}} = +0.50$ because at higher P_{tot} the maximum TiO and VO abundances both coincide with the condensation temperatures of Ca titanates, as illustrated in Figures 3 and 4. But at $\log P_{\mathrm{tot}} < +0.5$, VO abundance maxima occur at lower *T* than TiO maxima, consistent with the observation of the VO maximum in a later spectral type. Total pressures smaller than $\log P_{\mathrm{tot}} = +0.50$ and the temperatures at which the TiO and VO maxima occur in Figures 3 and 4 are consistent with the model atmospheres for late-M dwarfs discussed by Tsuji et al. (1996a).

The maximum abundances of TiO at $\log P_{\mathrm{tot}} < +0.50$ are indicated by the curve "TiO max.," which is positioned at 2010 K (Fig. 3). This maximum is in the region bordered by the contours where $\log X(\mathrm{TiO}) = -6.9$. The upper *T* limit of $\sim$2245 K for this region is relatively independent of P_{tot}. The lower *T* limits for $\log X(\mathrm{TiO}) \geq -6.9$ depend on P_{tot} and are constrained by condensate formation to be 1964 K at 1 bar and 1909 K at $10^{-0.5}$ bars (see § 6). Thus, the maximum TiO abundances occur between 1964 K (1 bar) and 2245 K.

At $\log P_{\mathrm{tot}} < +0.50$, VO maximum abundances occur very close to the Ca titanate condensation curve (Fig. 4). For example, the maximum VO abundances are at 1961 K (1 bar) and 1906 K (0.316 bars) and are only a few degrees higher than the Ca titanate condensation curve. The wedge-shaped region where VO mole fractions are $\geq 10^{-8}$ has a

pressure-independent upper limit of ~1970 K and lower limits of 1950 K (at 1 bar) and ~1865 K (at 0.316 bars). Thus, maximum VO abundances occur between 1950 K (1 bar) and 1970 K.

Using these results, the temperature for the TiO maximum at M8 is placed at 2010 K, with an upper limit of 2245 K. The temperature for the VO maximum at M9 is placed at 1960 K (at 1 bar), with an upper limit of 1970 K.

At the beginning of the L sequence, TiO and VO bands are weakening, which implies lower VO and TiO gas abundances. As discussed above, lower T-limits to the TiO and VO maxima depend on $P_{\rm tot}$ because these limits are constrained by the Ca titanate condensation temperatures. Then the temperatures at the beginning of the L sequence must be lower than the condensation temperature of the first Ti-bearing condensate and lower than those indicated from the lower temperature limits of the VO maximum abundance region. At 1 bar, this is at 1950 K. The TiO abundances drop once Ca titanates condense, and TiO gas is only ~10% of all Ti (Fig. 1) once gehlenite condensation begins at ~1910 K (at 1 bar). At this temperature, VO is not yet that strongly depleted, and VO gas contains about 60% of all vanadium. The much steeper decrease in TiO gas abundances (than that of VO gas) with decreasing temperature is seen in a comparison of Figures 3 and 4. For example, at 1 bar TiO abundances drop ~5 orders of magnitude from the maximum abundances at 2010–1500 K, while the corresponding drop in VO abundances is only ~3 orders of magnitude. These results for the oxide abundances resemble the measured TiO and VO band indexes as a function of spectral type shown by Kirkpatrick et al. (1999, 2000) and Martin et al. (1999). Their diagrams show a much stronger decline of TiO from its maximum at M8 to the early spectral types L0–L2, while VO decreases more gradually from its maximum at M9 to L4–L5. Considering these limited constraints, the temperatures at the beginning of the L sequence are tentatively placed at ~1910 K for L0.

The temperatures here are to be understood as a "chemical temperature scale," and these temperatures reflect lower limits to the effective temperatures. The effective temperatures of M and L dwarfs depend on atmospheric models, for which several different approaches currently exist (see Ackerman & Marley 2001; Allard et al. 2001; Tsuji 2002). In the atmospheric models, the emitting (photospheric) region, which defines $T_{\rm eff}$, can vary by several scale heights depending on wavelength. The TiO and VO observations at different wavelength could correspond to the lower temperatures above the photospheric region so that the "chemical temperatures" obtained from the TiO and VO chemistry would indicate lower limits to effective temperatures. However, the effective temperatures remain dependent on the atmospheric models, while the chemistry combined with existing observations more uniquely constrains a pressure and temperature set for the late-M and early-L subtypes and possibly for the later L and T dwarfs as well.

The temperature estimates of 2010 K (M8), 1960 K (M9), and 1910 K (L0) given here are at the lower temperature range discussed for the M/L transition. Kirkpartick et al. (1999, 2000) adopt $T_{\rm eff} \sim 2000$ K for L0. Tsuji et al. (1996a) and Jones & Tsuji (1997) derive $T_{\rm eff} \sim 2200$ K for M8 and ~2000–2100 K for M9 dwarfs, which is closer to the temperatures adopted by Kirkpatrick et al. (1999, 2000) for the M/L transition.

Martin et al. (1999) use results from Basri et al. (2000) to place $T_{\rm eff} \sim 2200$ K at L0. Basri et al. (2000) use the resonance absorption lines of Rb and Cs to derive effective temperatures for late-M and L dwarfs. Their temperatures of ~2300–2500 K for M9 and ~2200 K for L0 are at the high end of the various T-estimates. Temperatures of 2300–2500 K for M9 are higher than expected from the TiO maximum abundance region (2245–2010 K in Fig. 3). It is not clear from the paper by Basri et al. (2000) if thermal ionization of Cs and Rb was properly accounted for. They state that the alkali metals (Li, Na, K, Cs, and Rb) remain neutral at temperatures below 3000 K. However, as can be seen from Figure 2 of Lodders (1999), this is the case only at extremely high total pressures (~1000 bars) but not at total pressures relevant to M and L dwarfs. Above 2300 K, a large fraction of total Cs and Rb are still present as monatomic ions; e.g., 76% of all Cs is present as Cs^+ at 2300 K and 1 bar. At this $P_{\rm tot}$, neutral Rb is more abundant than Rb^+ only below ~2350 K, and neutral Cs is more abundant than Cs^+ only below ~2060 K (see Lodders 1999). If the abundances of neutral Cs and Rb were overestimated by Basri et al. (2000), lower T would be necessary to fit their observed Rb and Cs lines. Alternatively, the gravity and hence the total pressure may be overestimated in the modeling by Basri et al (2000), who note that their $T_{\rm eff}$-estimates are as much as 300 K higher when $\log g = 4.5$ is used instead of $\log g = 5.0$. If lower gravity applies, their temperatures for M9 would reduce to 2000–2200 K. The Allard/Hauschildt models used by Basri et al. (2000) were also used by Schweitzer et al. (2001) to fit observed spectra of late-M and early-L dwarfs. The low-resolution fits yield 2000–2100 K (at $\log g = 6.0$) for their two M9.5 objects, and high-resolution fits to the alkali lines give 1900–2000 K (for $\log g = 5$–6) for the same objects. These T-estimates are within the T-range suggested from the chemistry here.

It is worth mentioning that the observation of neutral monatomic Cs and Rb itself is in support of lower temperatures. The increasing strengths of the neutral alkali lines of Cs and Rb beginning near the M/L transition are in part caused by making the atmosphere more transparent because the major opacity sources TiO and VO begin to disappear. However, in order to see neutral Rb and Cs, they have to be present in sufficient amounts to begin with. As just noted above, neutral Cs is more abundant than Cs^+ only below 2060 K, which supports the relatively low temperature estimate of 2010 K here.

9. CONCLUSIONS

The first Ti-bearing condensates at total pressures relevant to late-type dwarfs are Ca titanates. The sequence is perovskite, $Ca_4Ti_3O_{10}$, and $Ca_3Ti_2O_7$ with increasing $P_{\rm tot}$. At lower temperatures, Ti oxides are stable when Ca is consumed by other condensates. The oxide sequence is Ti_2O_3, Ti_3O_5, and Ti_4O_7 with decreasing temperature. The stability of the different titanates and Ti oxides as a function of T and $P_{\rm tot}$ depends on the stability regions of Ca-Al–bearing condensates (corundum, hibonite, grossite, gehlenite, spinel, and akermanite). Removal of TiO gas by higher titanates ($Ca_4Ti_3O_{10}$ and $Ca_3Ti_2O_7$) is more effective than that by perovskite condensation.

Vanadium condensation chemistry is closely related to that of titanium because vanadium condenses into solid solution with Ti-bearing condensates. Condensation of pure

VO would occur after Fe metal condensation, which is inconsistent with the observed decrease in VO-band strengths at the M/L dwarf transition before FeH bands decline around the cooler type L3.

Computed TiO and VO gas abundances are used to estimate temperatures for late-M dwarfs. The maximum of TiO abundances indicates a *P*-independent temperature of 2010 K (with an upper limit of 2245 K) for M8, where TiO band strengths reach their maximum. The VO gas abundances place the *P*-dependent temperature estimates for M9 near 1960 K (at 1 bar). The temperature at the beginning of the L sequence is tentatively placed at ~1910 K for L0.

I thank Bruce Fegley for discussions and valuable insights. Comments by the referee and additional comments by T. Geballe and M. Marley are appreciated. This work was supported by NSF grant AST 00-86487 and NASA grant NAG5-11958.

APPENDIX

In § 5 it is noted that the differences between the computed Ti condensation sequence in this work and those by Burrows & Sharp (1999) and Allard et al. (2001) likely stem from the use of erroneous thermodynamic data for Ti_3O_5 by the two groups. Burrows & Sharp (1999) and Allard et al. (2001) draw a large set of thermodynamic data from Sharp & Huebner (1990, hereafter SH90). However, some of the data given in SH90 are inaccurate. SH90 list polynomial fit coefficients derived from fitting tabulated Gibbs free energy data as a function of temperature. The general form of their polynomial is $\Delta G(T) = a/T + b + cT + dT^2 + eT^3$.

SH90 use monatomic gases as the reference state so that for each compound A_xB_y the Gibbs free energy is given for the reaction $x\mathrm{A}\ (\mathrm{gas}) + y\mathrm{B}\ (\mathrm{gas}) = \mathrm{A}_x\mathrm{B}_y$. In the literature such as the JANAF tables (Chase et al. 1985), the Gibbs free energy is given with respect to the elements in their reference states (i.e., solid, liquid, or gas). Therefore, SH90 converted JANAF data (or other literature data as appropriate) to their chosen reference state of monatomic gases. In the following comparison, all data were also converted to this reference state.

An easy way to check the quality of a polynomial fit to the actual literature data is to plot the difference of the Gibbs free energy data (literature − polynomial fit) as a function of temperature. Such a plot is given in Figure 5 for Ti_3O_5, Ti_2O_3, Ti_4O_7, and $CaTiO_3$. If the polynomial fit accurately reproduces the literature data, the difference should plot along the horizontal zero line. If the difference is positive, the polynomial makes a compound more stable, while a negative difference makes the compound less stable. The next sections discuss the data in Figure 5.

A1. Ti OXIDES: Ti_3O_5, Ti_2O_3, AND Ti_4O_7

A fit using the polynomial fit coefficients given by SH90 to the tabulated Gibbs free energy data of Ti_3O_5 (solid) does not correctly reproduce the Gibbs free energy data of Ti_3O_5 (α, β, or liquid) listed in the JANAF tables, which is easily seen from Figure 5. The Ti_3O_5 curve shows positive and negative deviations, which means that the data from the polynomial fit make Ti_3O_5 more stable (positive deviation) or less stable (negative deviation) than expected from the literature.

Above 1800 K, the Gibbs energy for Ti_3O_5 computed from the polynomial given by SH90 deviates more and more from the values given in the JANAF tables. The results from the polynomial translate to higher Ti_3O_5 stability (i.e., more negative Gibbs free energy than listed in JANAF), which is likely the reason why Burrows & Sharp (1999) find Ti_3O_5 as the initial condensate in objects like G1 229B. This effect could be compounded if Burrows & Sharp (1999) used perovskite data from Turkdogan (1980), as indicated in SH90 (see § A2 below).

Below 1800 K, the Gibbs free energy from the fit by SH90 makes Ti_3O_5 less stable (less negative Gibbs free energy than listed in JANAF) down to ~700 K. The negative deviations from the JANAF data are largest around 1300–1400 K, which is the temperature region for which the condensation sequence Ti_2O_3-Ti_3O_5-Ti_4O_7 is identified here (~1700 to ~1300 K; see Figs. 1 and 2). Thus, if Burrows & Sharp (1999) and Allard et al. (2001) used Ti_3O_5 data from SH90, they likely did not find Ti_3O_5 in this temperature region because the Gibbs free energy from the polynomial fit makes Ti_3O_5 less stable.

The Gibbs free energies of Ti_2O_3 (solid; 1) and Ti_4O_7 (solid; 1) from the polynomial fit coefficients of SH90 agree with the data in JANAF within ± 4 kJ mol^{-1}, which should not significantly alter the results. However, the fits poorly match the data in the JANAF tables above 2000 K. This illustrates that extrapolated thermodynamic properties from polynomial fits are unreliable and that such fits can be used only for the temperature range for which the original data were fitted.

A2. PEROVSKITE

The comparison of perovskite in Figure 5 is for the data from the fit coefficients in SH90 and the data given in Robie & Hemingway (1995). The Gibbs free energy data in Robie & Hemingway (1990) agree within 2 kJ mol^{-1} with the data given in Robie & Waldbaum (1968), which is one of the data sources of SH90. However, SH90 use perovskite data from Turkdogan (1980), who gives a linear fit for the Gibbs free energy of the reaction of perovskite to the respective oxides as a function of temperature valid for the *T*-range of 298–1673 K. Turkdogan (1980) notes that these linear fits are good only as long as the difference in heat capacities of the reactants and products remains about constant over the temperature range of the fit. However, linear fits to the Gibbs free energy over a wide temperature interval should be avoided.

SH90 use the linear fit for the reaction as given by Turkdogan (1980) and combine these data with their polynomial fit coefficients of CaO and TiO_2 to obtain the coefficients for perovskite formation from the monatomic gases. A combination of the reactions I–III shown in Table 3 gives the desired reaction IV for perovskite. SH90 then used the combination of fit coefficients for reactions I–III to obtain the fit coefficients for the Gibbs free energy of reaction IV, as shown in Table 4.

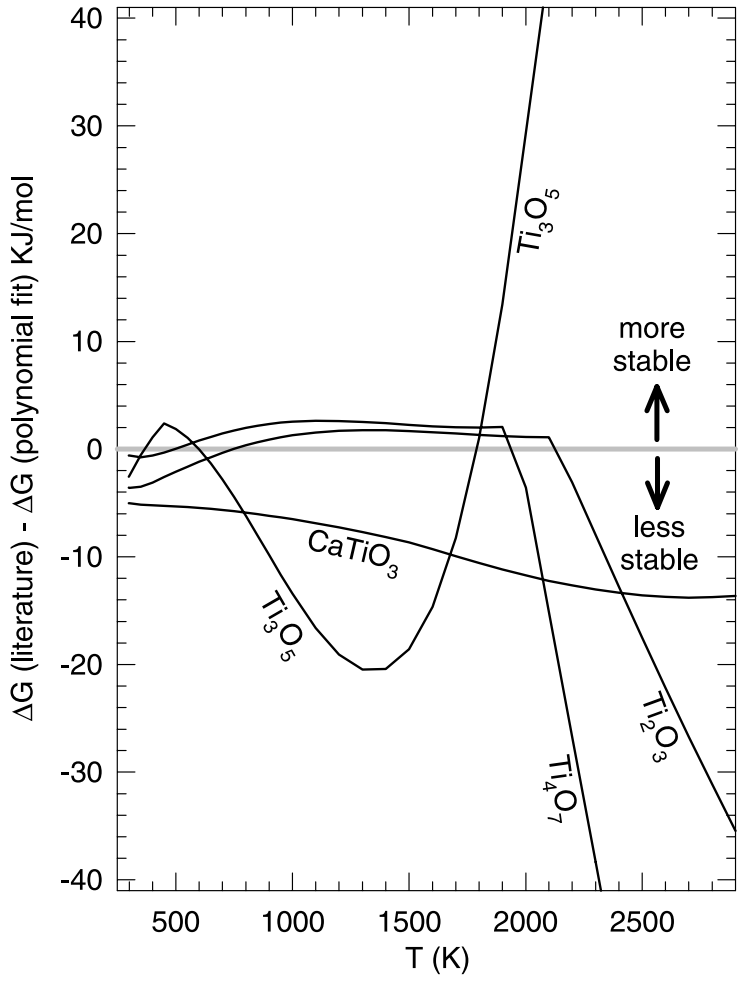

FIG. 5.—Differences between the literature Gibbs free energy data and the data obtained from the polynomial fit coefficients given by SH90 as a function of temperature for titanium oxides and perovskite. If the polynomial fit accurately reproduces the literature data, the difference should plot along the horizontal zero line. If the difference is positive, the polynomial makes a compound more stable, while a negative difference makes the compound less stable.

TABLE 3

REACTIONS

Number	Reaction	Reference
I	$CaTiO_3 = CaO$ (solid) + TiO_2 (solid)	1
II	Ca (gas) + O (gas) = CaO (solid)	2
III	Ti (gas) + 2O (gas) = TiO_2 (solid)	2
−I + II + III = IV	Ca (gas) + Ti (gas) + 3O (gas) = $CaTiO_3$ (solid)	

REFERENCES.—(1) Turkdogan 1980; (2) SH90.

TABLE 4

FIT COEFFICIENTS

NUMBER	FIT COEFFICIENTS (kcal mol^{-1})				
	a	*b*	*c*	*d*	*e*
I	0	1.91000×10^4	0.8	0	0
II	-4.65399×10^3	-2.54265×10^5	6.72853×10^1	-1.67646×10^{-3}	1.10392×10^{-7}
III	1.65647×10^4	-4.56962×10^5	1.09445×10^2	-1.16984×10^{-3}	0
−I + II + III = IV	1.19107×10^4	-7.30327×10^5	1.75930×10^2	-2.84630×10^{-3}	1.10392×10^{-7}

This is a questionable scheme of treating thermodynamic data because the coefficients *a*, *d*, and *e* come only from the CaO and TiO_2 fits that were done from JANAF data, and the fits cover different temperature ranges. It would have been better for SH90 to have obtained a polynomial fit to Gibbs free energy data that included heat-capacity variations. The inclusion of heat-capacity variations with temperature is important because Figure 5 shows that the perovskite data from the polynomial by SH90 increasingly deviate from the literature data with increasing temperature. At 298.15 K, the data from the polynomial agree within ± 3 kJ mol^{-1} with the data in Robie & Hemingway (1995) and those given by Robie & Waldbaum (1968). However, at 2000 K, the polynomial makes perovskite less stable by ~ 12 kJ mol^{-1}. Thus, if Burrows & Sharp (1999) used the perovskite data from SH90, the use of "less stable" perovskite also added to the effect that they identified Ti_3O_5 instead of perovskite as the initial condensate in brown dwarfs.

It is also not clear why SH90 used perovskite data from Turkdogan (1980) and not the data from Robie & Waldbaum (1968), which they use as a source for other compounds. Robie & Waldbaum (1968) contains better Gibbs free energy data than obtained from a linear fit for perovskite, as does the reference Robie, Hemingway, & Fisher (1978), which was also available at the time when Sharp & Huebner did their 1990 paper. Even if the combination of fit coefficients were reliable and the effects of heat-capacity variations were negligible, results computed using perovskite data from SH90 are suspect, especially if extrapolated above the range of the original linear fit of 1673 K.

REFERENCES

Ackerman, A. S., & Marley, M. S. 2001, ApJ, 556, 872
Allard, F., Hauschildt, P. H., Alexander, D. R., Tamanai, A., & Schweitzer, A. 2001, ApJ, 556, 357
Basri, G., Mohanty, S., Allard, F., Hauschildt, P. H., Delfosse, X., Martin, E. L., Forveille, T., & Goldman, B. 2000, ApJ, 538, 363
Burgasser, A. J., et al. 2002, ApJ, 564, 421
Burrows, A., & Sharp, C. M. 1999, ApJ, 512, 843
Chase, M. W., Davies, C. A., Downey, J. R., Frurip, D. J., McDonald, R. A., & Syverud, A. N. 1985, J. Phys. Chem. Ref. Data, 14, 1
Ebel, D. S., & Grossman, L. 2000, Geochim. Cosmochim. Acta, 64, 339
Fegley, B., & Lodders, K. 1994, Icarus, 110, 117
———. 1996, ApJ, 472, L37
Geballe, T. R., Saumon, D., Leggett, S. K., Knapp, G. R., Marley, M. S., & Lodders, K. 2001, ApJ, 556, 373
Geballe, T. R., et al. 2002, ApJ, 564, 466
Jones, H. R. A., & Tsuji, T. 1997, ApJ, 480, L39
Kirkpatrick, J. D., et al. 1999, ApJ, 519, 802
———. 2000, AJ, 120, 447
Kornacki, A. S., & Fegley, B. 1984, J. Geophys. Res., 89 (Suppl.), B588
———. 1986, Earth Planet. Sci. Lett., 79, 217
Lodders, K. 1999, ApJ, 519, 793
Lodders, K., & Fegley, B. 1998, The Planetary Scientist's Companion (New York: Oxford Univ. Press)
———. 2002, Icarus, 155, 393
Martin, E. L., Delfosse, X., Basri, G., Goldman, B., Forveille, T., & Zapatero Osorio, M. R. 1999, AJ, 118, 2466
Nakajima, T., Oppenheimer, B. R., Kulkarni, S. R., Golimowski, D. A., Matthews, K., & Durrance, S. T. 1995, Nature, 378, 463
Robie, R. A., & Hemingway, B. S. 1995, US Geological Survey Bull. 2131
Robie, R. A., Hemingway, B. S., & Fisher, J. R. 1978, US Geological Survey Bull. 1452
Robie, R. A., & Waldbaum, D. R. 1968, US Geological Survey Bull. 1259
Schweitzer, A., Gizis, J. E., Hauschildt, P. H., Allard, F., & Reid, I. N. 2001, ApJ, 555, 368
Sharp, C. M., & Huebner, W. F. 1990, ApJS, 72, 417
Tsuji, T. 2002, ApJ, 575, 264
Tsuji, T., Ohnaka, K., & Aoki, W. 1996a, A&A, 305, L1
Tsuji, T., Ohnaka, K., Aoki, W., & Nakajima, T. 1996b, A&A, 308, L29
Turkdogan, E. T. 1980, Physical Chemistry of High Temperature Technology (New York: Academic)